Tailoring the Lasing Modes in Semiconductor Nanowire Cavities Using Intrinsic Self-Absorption

ARTICLE *in* NANO LETTERS · FEBRUARY 2013

Impact Factor: 13.59 · DOI: 10.1021/nl304362u · Source: PubMed

4 AUTHORS, INCLUDING:

Qihua Xiong
Nanyang Technological University
166 PUBLICATIONS **3,984** CITATIONS
SEE PROFILE

Tze Chien Sum
Nanyang Technological University
144 PUBLICATIONS **3,513** CITATIONS
SEE PROFILE

NANO LETTERS

Letter

pubs.acs.org/NanoLett

Tailoring the Lasing Modes in Semiconductor Nanowire Cavities Using Intrinsic Self-Absorption

Xinfeng Liu,[†,⊥,∥] Qing Zhang,[†,∥] Qihua Xiong,[*,†,‡] and Tze Chien Sum[*,†,§,⊥]

[†]Division of Physics and Applied Physics, School of Physical and Mathematical Sciences, Nanyang Technological University, Singapore 637371

[‡]Division of Microelectronics, School of Electrical and Electronic Engineering, Nanyang Technological University, Singapore 639798

[§]Energy Research Institute @ NTU (ERI@N), Nanyang Technological University, 50 Nanyang Drive, Singapore 637553

[⊥]Singapore-Berkeley Research Initiative for Sustainable Energy (SinBeRISE), 1 Create Way, Singapore 138602

Supporting Information

ABSTRACT: Understanding the optical gain and mode-selection mechanisms in semiconductor nanowire (NW) lasers is key to the development of high-performance nanoscale oscillators, amplified semiconductor/plasmon lasers and single photon emitters, and so forth. Modification of semiconductor band structure/bandgap through electric field modulation, elemental doping, or alloying semiconductors has so far gained limited success in achieving output mode tunability of the NW laser. One stifling issue is the considerable optical losses induced in the NW cavities by these extrinsic methods that limit their applicability. Herein we demonstrate a new optical self-feedback mechanism based on the intrinsic self-absorption of the gain media to achieve low-loss, room-temperature NW lasing with a high degree of mode selectivity (over 30 nm). The cadmium sulfide (CdS) NW lasing wavelength is continuously tunable from 489 to 520 nm as the length of the NWs increases from 4 to 25 μm. Our straightforward approach is widely applicable in most semiconductor or semiconductor/plasmonic NW cavities.

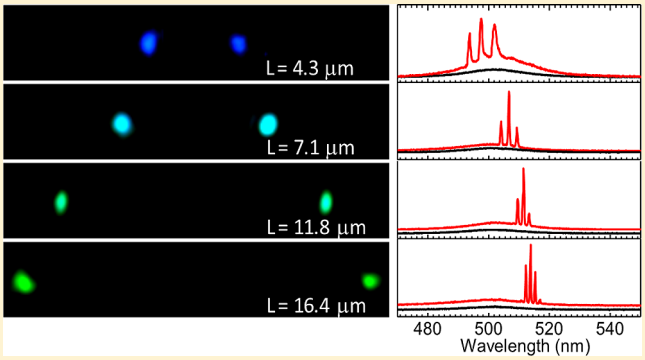

KEYWORDS: *Cadium sulfide, nanowire cavity, Urbach tail, waveguide, lasing*

Single crystalline semiconductor Fabry–Pérot or whispering gallery nanowire (NW) cavity possessing naturally formed flat facets for good optical feedback is an ideal gain media for light amplification.[1−10] They are considered as one of the most important and promising routes to realizing miniaturized nanolasers and amplifiers.[11−13] Recent groundbreaking work on utilizing semiconductor NW cavities to compensate the damping loss and amplify the collective electron oscillations in plasmon nanocavities has kindled even greater interests in this field.[2,13,14] For practical applications, the ability to tailor the NW cavity mode is essential for developing multicolor miniaturized lasers, and critical for optimizing the resonant energy transfer between the cavity and the coupled system.[15]

For a II–VI or III–V NW Fabry–Pérot cavity, it is generally accepted that the output laser wavelength is determined by the bandgap of semiconductor NW.[11] To date, there is only limited success in tuning the optical cavity modes through (a) electric field modulation and (b) elemental doping of the semiconductors.[6,9,16] In the former approach where the bandgap is modulated via the Franz-Keldysh or Stark effects, the NW cavities are highly susceptible to damage and only narrow tunability around 10 nm is demonstrated;[17] in the later approach, the NW cavities are prone to structural defects induced by the dopants, thereby restricting the cavity gain. Though broadband tunable lasing wavelengths spanning 100 nm or more have been demonstrated in ternary semicondutor NW cavities,[18] cavity gain is however limited by the structural defects formed during the growth phase.[7,16] Use of extrinsic optical feedback such as photonic crystals to achieve better mode selectivity is another approach. However, the high-cost and complicated fabrication required, together with the weak coupling and the high optical losses between the two different cavities would offset any advantages.[19,20] Achieving low loss cavity modes with a high degree of mode selectivity, while not compromising on the quality and integrity of the nanostructures is therefore an important and yet nontrivial challenge to overcome.

In this work, we present a new approach based on utilizing the intrinsic self-absorption at the Urbach tail states to tailor the NW cavity lasing wavelength of semiconductor nanostructures. Importantly, this novel method allows one to achieve excellent mode selectivity spanning more than 30 nm with high cavity

Received: November 27, 2012
Revised: January 22, 2013
Published: February 8, 2013

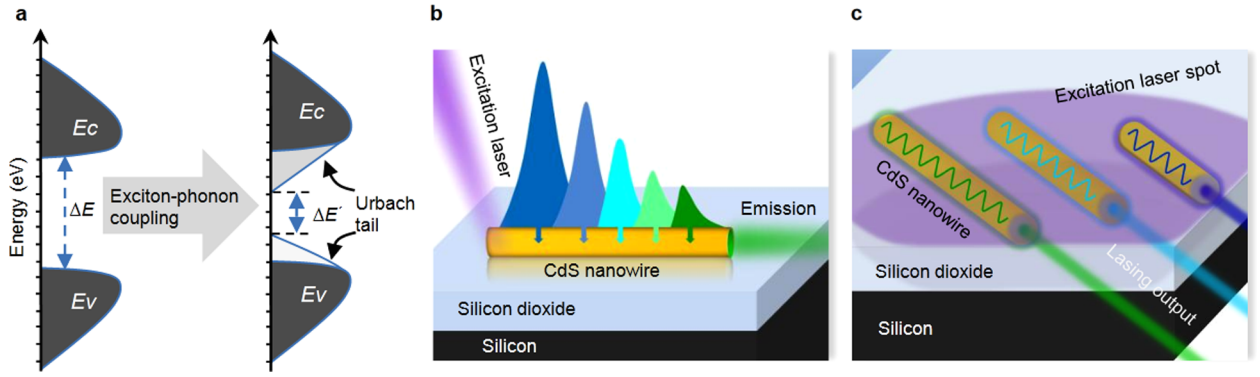

Figure 1. Schematics of the Urbach tails at the band edges and the length-dependent lasing mode selections for CdS nanowires (NWs). (a) In undoped semiconductors, exciton−phonon coupling distort the electron−lattice interaction, resulting in a tailing of the states at the adsorption edges known as the Urbach tail. (b) The CdS NW on silicon substrate with a layer of SiO_2 of 300 nm. When excited with laser pulses at one end (left end), the exciton−polaritons propagate inside the NWs and undergo scattering by the surface defects/phonons and subsequently self-absorption at the Urbach tail (see the Supporting Information Figure S1 for more details of the exciton−polariton absorption). (c) Various output lasing colors are observed at the end facets of CdS NWs with different lengths (but with comparable diameters) that are placed on a silicon substrate with a 300 nm layer of SiO_2 for photoexcitation.

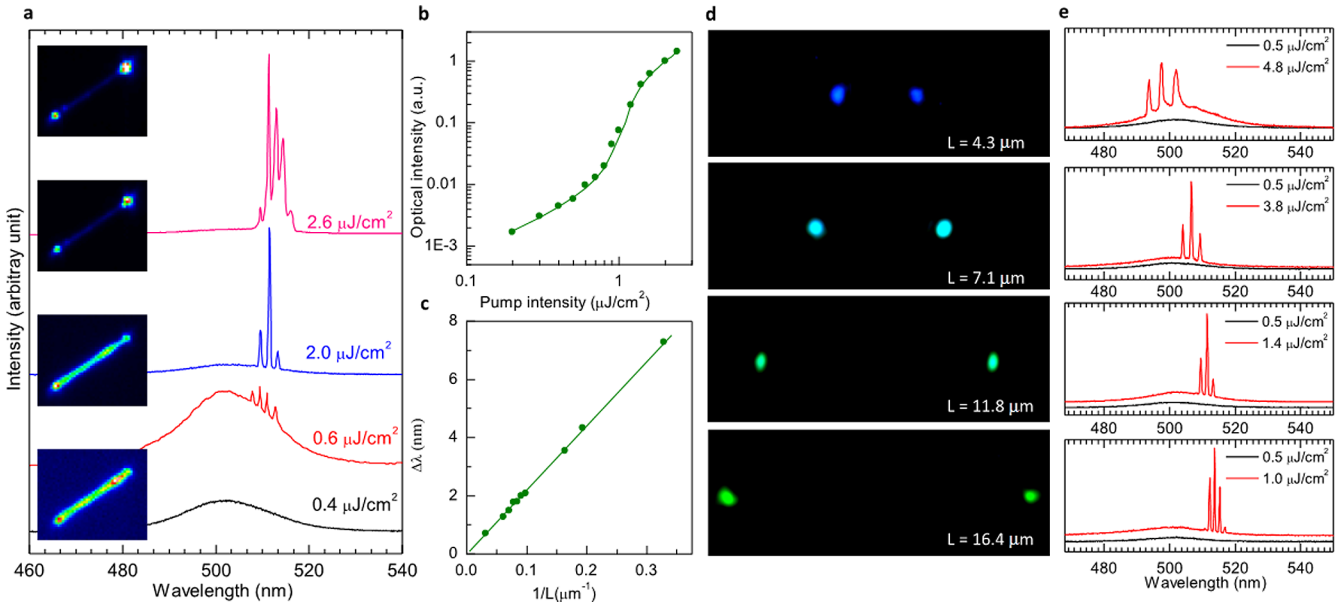

Figure 2. Nanowire length-dependence lasing modes for CdS nanowires (NWs). (a) Emission spectra for a 12.8 μm long CdS NW with a diameter of 265 nm photoexcited with different pump fluence (0.4 to 2.6 $\mu J/cm^2$), illustrating the transition to lasing action. Insets show the far-field images of the same NW under different pump intensities. (b) The logarithmic plot of the integrated PL intensity as a function of pump fluence with a fit of the data using the model in ref 32 (eq 23), green line. (c) Mode spacing $\Delta\lambda$ under lasing conditions versus NW length for 10 independent NWs. Red spheres are experimental data points and the red line is a linear fit of the data. (d) Optical images of four individual CdS NWs with different lengths but with comparable diameter (~250 (±20) nm) undergoing lasing. The NW lengths are 4.3, 7.1, 11.8, and 16.4 μm, respectively. (e) The corresponding emission spectra of the four NWs presented in panel d under lasing action (red spectra). The nonlasing (PL) spectra are included for comparison (black spectra).

gain in highly crystalline, nominally undoped CdS NWs. In undoped polar semiconductors, the fluctuation in electronic energy bands arising from the exciton−phonon coupling (i.e., Fröhlich interaction) can induce an extension of the density of states from the bandedge into the bandgap.[21−23] Optical transitions (with lower energies) to these extended states give rise to an exponential tail near the fundamental optical absorption edge known as the Urbach tail (see Figure 1a).[24,25] These transitions are significantly enhanced in one-dimenional (1-D) nanostructures due to the stronger exciton−phonon coupling strength compared to their bulk counterparts.[26,27] Herein, the representative CdS NW system present us with an excellent 1-D model nanostructure system to demonstrate the physics underpinning this novel method.

When the NW cavities are optically excited, polaritons waveguide along the long axis of NW (see Figure S1 in Supporting Information). Upon scattering into the lower polariton branch by the NW surface, the exciton−polaritons can lose their energy efficiently through scattering with phonons (Figure 1b) and absorption can occur.[28−31] When the energy of the propagating polaritons become lower than the bottom of Urbach tail, there will be no optical absorption and the polaritons will undergo further energy dissipation through phonon scattering as they propagate along the cavity. At the

dx.doi.org/10.1021/nl304362u | Nano Lett. 2013, 13, 1080−1085

end-facets, the polaritons are reconverted back to photons with an asymmetric energy distribution whose spectrum exhibits a low energy tail. Consequently, the output longitudinal cavity modes of the NW, selected at the end-facets, are located in the lower energy side of the photoluminescence (PL) emission peak. The energy loss of the polaritons is mainly dependent on the length of the waveguide for a given NW cavity, such as along the long-axis of the NW cavity. With increasing NW lengths, the energy loss of the polaritons will be increased. From this exciton−polariton picture, it is clear that the cavity modes will be red shifted (Figure 1c).

Figure 2a displays the PL spectra of a single CdS NW (diameter ∼260 nm, length ∼12.8 μm) as a function of laser pump intensity (I_{ex}). A schematic of the optical measurement system is given in the Supporting Information (see Figure S2). The four spectra in Figure 2a, obtained with increasing pump fluence, illustrate the transition from spontaneous emission (0.4 μJ/cm^2) via amplified spontaneous emission (0.6 μJ/cm^2) to full lasing action (2.0 and 2.6 μJ/cm^2). Figure 2b shows the output power on a log−log scale with a multimode laser model,[32] which gives a threshold fluence of ∼0.76 μJ/cm^2. When I_{ex} < 0.52 μJ/cm^2, the spectrum is broad and featureless and centered around 502 nm with a full width at half-maximum (fwhm) of 20 nm. The PL emission is essentially isotropic along the length of the NW (see inset, bottom image of Figure 2a). When I_{ex} is increased to 0.6 μJ/cm^2, additional sharp emission lines (with fwhm ∼0.4 nm) appear above the broad near-band edge emission peak. These peaks correspond to the longitudinal cavity modes that are formed when the propagation losses are compensated by gain, allowing the photonic modes to resonate between the reflective NW end-facets.[33] As the pump intensity approaches the lasing threshold, the emission output exhibits a superlinear increase (Figure 2b), which is expected. At I_{ex} > 0.78 μJ/cm^2, the spectrum is dominated by the sharp emission lines with an intensity several orders of magnitude greater than the spontaneous emission background.[34] From transient PL measurements, the dominant fast recombination lifetime of around 10 ps (see Figure S3 in Supporting Information) is also an indication of the lasing behavior.[35−37] Upon lasing, the output power exhibits a linear dependence with the pump fluence and the emission wavelengths are concentrated in a narrow range (505 nm < λ < 512 nm). The mode spacing of the observed sharp emission lines $\Delta\lambda$ is measured to be inversely proportional to the NW length L (Figure 2c), which is in good agreement with the theoretical equation $\Delta\lambda = (1/\lambda)[(\lambda^2/2)(n - \lambda dn/d\lambda)^{-1}]$ for a Fabry−Pérot cavity, where n is the index of refraction at wavelength λ.[38]

Next, we highlight the effect of the CdS NW length on the lasing modes. To correct for any influence of the NW diameter on the measurements, four CdS NWs with comparable diameter of D ∼ 250 (±20) nm were chosen and these NWs have lengths of 4.3, 7.1, 11.8, and 16.4 μm. The excitation laser spot size was beam expanded to permit the full coverage of the whole NW during the experiment. Moreover, a large pump spot ensures efficient energy injection and avoids possible damage to the samples at high pump fluences above the lasing threshold. It should also be highlighted that the difference of laser spot size does not significantly influence the lasing modes in the NWs, as shown in the Supporting Information (Figures S4 and S5). Figure 2d shows the real color optical images of these four NWs photoexcited with above lasing threshold fluence. The lasing wavelengths emitted from the two end-facets show distinct colors. As the NW length increases from 4.3 to 16.4 μm, the lasing wavelength changes from blue (495 nm) to green (516 nm). The corresponding spectra of their lasing output were recorded and the nonlasing PL spectra were also plotted for comparison (Figure 2e). The broad spontaneous emission bands of these individual NWs are symmetrically centered at 502 nm, suggesting that they have a common band gap energy. However, the position of the dominant lasing mode is 498, 508, 512, and 518 nm for NW lengths of 4.3, 7.1, 11.8, and 16.4 μm, respectively. These observations indicate that the mode-tunability of the NW cavities can be achieved by tuning the NW length.

To elucidate the influence of NW dimensions (length and diameter) on the lasing wavelengths, extensive measurements on three groups of NWs with diameters of 400 ± 30 nm (blue squares), 300 ± 30 nm (purple circles), and 200 ± 30 nm (green triangles) were performed (Figure 3a). From these experimental data, we can deduce that (1) the lasing wavelength redshifts with increasing NW length for NWs of a

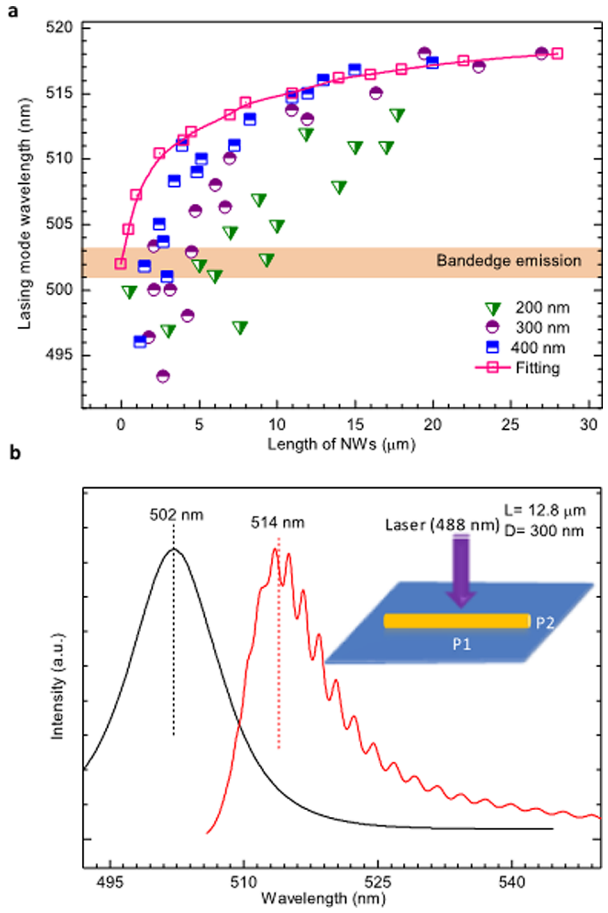

Figure 3. Nanowire length and diameter dependent lasing mode. (a) The lasing mode wavelengths of CdS NWs as a function of NW length from 1 to 35 μm. The NW diameters are 400 (±30) nm (blue squares), 300 (±30) nm (purple circles), and 200 (±30) nm (green triangles). The hollow pink squares represent the calculated lasing modes after correcting for self-absorption using eq 1. The solid pink line is merely a guide for the eye. The deviation of the experimental data from theory is due to the band filling effects, which is more apparent in the shorter or narrower NWs. (b) Normalized PL spectra detected at the excitation position P1 (black line) and at the right end P2 (red line) of the NW. Inset shows the experimental configuration.

dx.doi.org/10.1021/nl304362u | Nano Lett. 2013, 13, 1080−1085

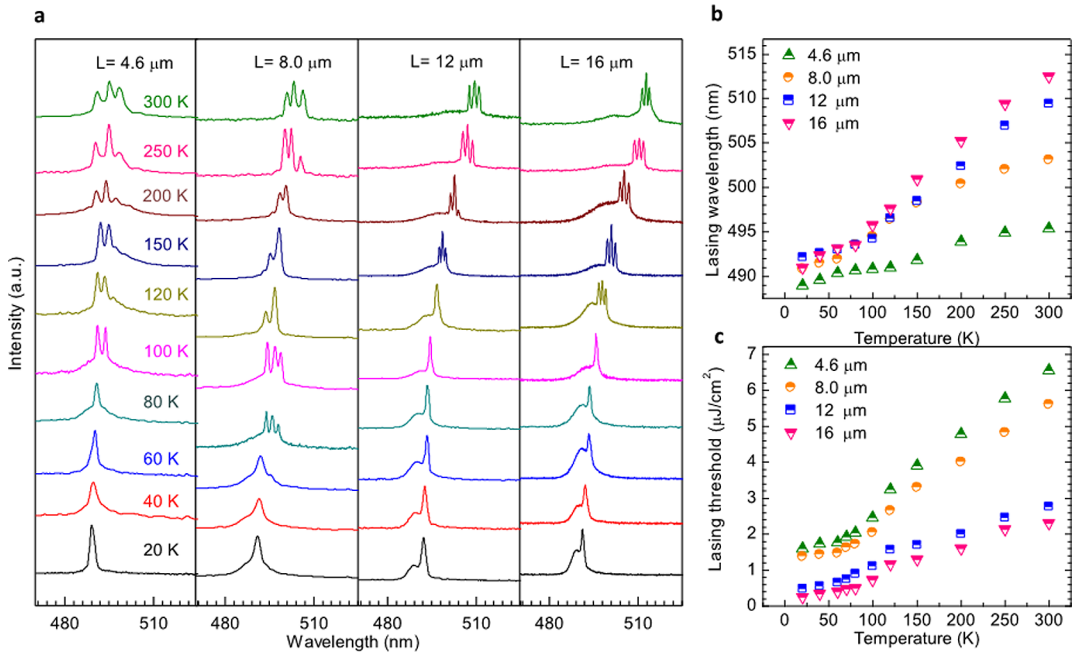

Figure 4. Temperature-dependent lasing properties of CdS nanowires. (a) Temperature-dependent lasing spectra recorded from four individual CdS NWs. The lengths of the NWs (from left to right) are 4.6, 8.0, 12, and 16 μm but with comparable diameter (~250 ± 20 nm). The temperature was varied from 20 to 300 K. The curves in the four subfigures are taken at the same temperature. (b) Temperature dependence of the most prominent lasing mode or the center-most peak (in the case of multiple peaks with comparable intensity) extracted from a. (c) Temperature dependence of the lasing threshold for the four CdS NWs.

specific diameter; (2) for a fixed NW length, the NW with a larger diameter exhibit a larger redshift; (3) for a fixed NW diameter, the redshift approaches a limit beyond a certain NW length; (4) for the shorter NWs (<10 μm), the lasing modes are located primarily at the high energy side of the band edge emission peak; and (5) for the thinner NWs (e.g., 200 nm diameter), the lasing modes exhibit a smaller red shift compared to the thicker NWs. Given that the PL emission plays a crucial role in the provision of seed photons for the gain buildup and the subsequent photon cascade, the optical self-absorption of the exciton−polaritons propagating along the NW cavity is therefore expected to have a strong bearing on the NW lasing modes. However, to our pleasant surprise intrinsic optical self-absorption alone could not satisfactorily account for some of the above phenomena, despite being a key factor in NW lasing, which we shall discuss in the following sections.

Theoretically, the absorption coefficient $\alpha(E)$ of a semiconductor with contributions from the Urbach rule[16,25,39] can be described by the following expressions

$$\alpha(E) = \begin{cases} A_0\sqrt{\dfrac{k_BT}{2\sigma}}\ \exp\left[\dfrac{\sigma}{k_BT}(E - E_{cr})\right], & E \geq E_g \\ A_0\ \exp\left[\dfrac{\sigma}{k_BT}(E - E_g)\right], & E < E_g \end{cases} \quad (1)$$

where A_0 is a constant, E_g is the band gap energy, k_BT is the thermal energy at room temperature, σ is a dimensionless phenomenological fitting parameter, the energy $E = h\nu$ with h being the Planck's constant, ν is the photon frequency, and $E_{cr} = E_g + k_BT/2\sigma$ is the crossover energy. To determine the parameters of σ and A_0 used in eq 1, a control experiment was also performed and more details of this control experiment and the fits are found in Figure S6 and S7 (see Supporting Information). Experimentally, a 488 nm continuous wavelength laser was focused at the middle of a NW and the confocal μ-PL spectra at the excitation position (P1) and to the right end (P2) of the NW were measured (Figure 3b). The PL detected at P1 has a peak around 502 nm, which is attributed to the band edge emission of the CdS NW (without any propagation loss). The PL emitted from P2 exhibits a series of periodic peaks (arising from the FP cavity) overlaid on an asymmetric main emission peak (at 514 nm). The 12 nm redshift and the asymmetry on the high energy side of the main emission peak are due to the reabsorption of the PL emission in the CdS NW cavity.

By substituting eq 1 to the material absorption equation, the peak positions of the calculated emission spectra after accounting for optical self-absorption is plotted in Figure 3a (pink hollow squares), see also Supporting Information Figure S6. Its trend clearly matches that of the experimental data and is located in the wavelength region where gain build-up occurs. These theoretical results concur with the experimental findings that the calculated spectra exhibit a significant redshift with increasing NW dimensions and the calculated redshift approaches saturation for a specific NW length. The excellent agreement between the experimental results and the theory validates that the PL and lasing redshift in these NWs do indeed originate from the optical self-absorption of the Urbach tail states.

In the above calculations, the propagation loss of each F−P mode arising from mode confinement in NWs with different lengths can be taken to be the same. This is because of the following reasons: (a) the NWs have diameters ranging from 200− 400 nm, which is larger than half the wavelength of the PL emission (490−530 nm) propagating inside the NW. Finite difference time domain (FDTD) simulations revealed that the modes are indeed well-confined inside the NW (see Supporting Information Figure S8). (b) Q-factor calculations showed that

dx.doi.org/10.1021/nl304362u | Nano Lett. 2013, 13, 1080−1085

the propagation losses of the different modes within the 30 nm range (498 to 520 nm) are comparable, see Supporting Information Figure S9. Furthermore, the NWs in our experiment are grown under the same conditions and exhibit a highly crystalline structure. Propagating losses from these NWs are therefore expected to be similar.

Despite the concurrence between theory and experiment in Figure 3a, the latter two phenomena (i.e., (4) and (5) discussed above) could not be adequately addressed by considering this optical self-absorption mechanism alone. In the case of (4), the lasing modes for the shorter NWs (<10 μm) are located at the high energy side of the emission peak, which is contrary to the understanding that optical self-absorption always result in a redshift of the lasing modes to the lower energy side of the emission peak. In the case of (5), the smaller redshift of the lasing modes in the thinner NWs (200 nm diameter) compared to the thicker NWs is also contrary to the understanding that the self-absorption-induced losses in the thinner NWs are more significant due to greater surface scattering. Nevertheless, temperature dependent NW lasing experiments (from 20 to 300 K, see Figure 4a) would allow us to unravel this seemingly disparate behavior and elucidate the intricacies of the NW lasing behavior, that is, comprising of an interplay of four effects: (i) the Varshni effect (red shifting); (ii) the phonon-mediated Urbach effect (red shifting); (iii) the phonon-mediated exciton−polariton adsorption (red shifting); and (iv) the band-filling effects (blue shifting).

The lasing wavelengths and pump-power thresholds as a function of temperature are extracted and plotted in Figure 4b,c, respectively. At 20 K, the lasing wavelengths of four different NWs (with length L = 4.6, 8.0, 12, and 16 μm and comparable diameters of 250 ± 20 nm) show little difference (i.e., 489 nm for L = 4.6 μm, and 491 nm for L = 16 μm). As the temperature increases to 300 K, the lasing wavelengths redshift as a result of the Varshni effect (i).[40] The wavelength shift per Kelvin (i.e., the slope) is much larger for the long NWs (~0.08 nm/K) compared to the short NWs (~0.02 nm/K). Furthermore, the phonon-mediated effects of (ii) and (iii) would be suppressed under low temperatures (e.g., experimental evidence of the narrowing of the Urbach tail width at lower temperatures is presented in the Supporting Information Figure S10). The influence of effect (iv) then becomes more evident from the results in Figure 4 at low temperatures.

Figure 4c clearly shows that the lasing threshold for the shorter NWs is ~3−4 times larger than those of the longer wires. For lasing to occur, the round-trip gain must be larger than the losses in the NW. The lasing threshold (assuming equal end-facet losses) is defined as $I_{th} \propto [1/(2L)]\ln(1/R^2)$, where L is the NW length, and R is the reflection coefficient.[41] At the lasing threshold (pump fluence, 10 μJ/cm^2), the carrier density inside the short NW (D, 250 nm, L, 4.6 μm) is estimated to be $n \sim 5 \times 10^{18}$ cm^3, sufficiently high for band-filling effects. At high pump intensity, there is a combined effect of carrier screening (blue shifting), band filling (blue shifting), and bandgap renormalization (red shifting).[41−43] Given the evident blueshift observed in our experiments, the former two effects dominate in our case. Lastly, the confinement losses (or mode intensity losses) in thin NWs is more significant than in the thick NWs.[33] Therefore, to achieve the lasing in thinner NWs, higher laser pump fluence is needed to compensate for these losses, resulting in higher photogenerated carrier densities. Hence, a larger blueshift of the lasing wavelengths in the thin NWs compared to the thick NWs is therefore expected. Such band filling effects on the NWs will account for the phenomena in (4) and (5), see Figure 3a.

In summary, we demonstrate for the first time a new optical self-feedback mechanism to achieve low-loss, room-temperature NW lasing with a high degree of mode selectivity over 30 nm. This is achieved through utilizing the intrinsic self-absorption at the Urbach tail states of semiconducting nanostructures. The variable lasing wavelength range, which is dependent on emission bandwidth, could also be further extended through tuning the NW emission properties. A detailed understanding of the physics that underpins the optical gain and mode-selection mechanisms in these semiconducting NWs is presented. We expect that this simple method can be easily extended to other semiconductors or plasmonic cavities to produce room-temperature miniaturized, multicolor lasers. The knowledge gained in this work will open up new approaches for the design of cavities or gain materials for large-scale and low-loss tunable lasers.

Methods. Single-crystal CdS nanowires (NWs) were synthesized by a simple vapor transport technique and subsequently dispersed onto a Si/SiO_2 substrate (300 nm thermal oxide).[44,45] The NW diameters were determined by atomic force microscopy (AFM) height measurement relative to the silicon substrates. The CdS NW lengths were determined from the SEM images. For femtosecond optical spectroscopy, the laser source was a Coherent Legend regenerative amplifier (150 fs, 1 kHz, 800 nm) that was seeded by a Coherent Mira oscillator (100 fs, 80 MHz). The 800 nm wavelength laser pulses were from the regenerative amplifier's output while the 400 nm wavelength laser pulses were frequency doubled from the 800 nm fundamental with a BBO crystal. The laser pulses were focused onto an individual CdS NW with a diameter of ~30 μm using a Nikon microscope equipped with a 50× objective (NA = 0.65). This 30 μm spot is produced with the aid of an external beam expander to allow coverage of the whole NW. The PL emission signal from the NW was collected by the same microscope objective in a backscattering configuration and recorded by a Photometrics CoolSNAP color camera to obtain the PL image. A 425 nm long pass filter was used to block the excitation laser. To obtain the PL spectra, the collected emission is collected by a Princeton Instrument spectrometer (PI Acton, Spectra Pro 2500i), dispersed by a grating of 600 g/mm and detected by a TE (thermoelectrically)-cooled charge coupled detector (CCD, PIXIS-400B); images were obtained with the same system by replacing the grating with a mirror. For low-temperature PL measurements, a liquid-helium-cooled microscopy cryostat system (Janis Research) was also used.

■ ASSOCIATED CONTENT

Ⓢ Supporting Information

Additonal figures and information. This material is available free of charge via the Internet at http://pubs.acs.org.

■ AUTHOR INFORMATION

Corresponding Author

*E-mail: (Q.X.) qihua@ntu.edu.sg; (T.C.S.) tzechien@ntu.edu.sg.

Author Contributions

‖These authors contribute to this work equally.

Notes

The authors declare no competing financial interest.

■ ACKNOWLEDGMENTS

T.C.S. acknowledges the support from the following research grants: NTU start-up grant (M58110068); Academic Research Fund (AcRF) Tier 1 − RG 49/08 (M52110082); Ministry of Education AcRF Tier 2 Grant MOE2011-T2-2-051 (M402110000). X.L. and T.C.S. also acknowledge the financial support by the Singapore National Research Foundation (NRF) through the Competitive Research Programme (CRP) under Project No. NRF-CRP5-2009-04 and the Singapore-Berkeley Research Initiative for Sustainable Energy (SinBeRISE) CREATE Programme. Q.X. acknowledges the support of this work from the Singapore National Research Foundation through NRF fellowship grant (NRF-RF2009-06), Ministry of Education via an AcRF Tier 2 Grant (MOE2011-T2-2-051), and start-up grant support (M58113004) from Nanyang Technological University (NTU).

■ REFERENCES

(1) Groblacher, S.; Hertzberg, J. B.; Vanner, M. R.; Cole, G. D.; Gigan, S.; Schwab, K. C.; Aspelmeyer, M. *Nat. Phys.* **2009**, *5*, 485−488.
(2) Oulton, R. F.; Sorger, V. J.; Zentgraf, T.; Ma, R. M.; Gladden, C.; Dai, L.; Bartal, G.; Zhang, X. *Nature* **2009**, *461*, 629−632.
(3) Johnson, J. C.; Choi, H. J.; Knutsen, K. P.; Schaller, R. D.; Yang, P. D.; Saykally, R. J. *Nat. Mater.* **2002**, *1*, 106−110.
(4) Heber, J. *Nature* **2009**, *461*, 720−722.
(5) Yan, R. X.; Gargas, D.; Yang, P. D. *Nat. Photonics* **2009**, *3*, 569−576.
(6) Kuykendall, T.; Ulrich, P.; Aloni, S.; Yang, P. *Nat. Mater.* **2007**, *6*, 951−956.
(7) Pan, A. L.; Zhou, W. C.; Leong, E. S. P.; Liu, R. B.; Chin, A. H.; Zou, B. S.; Ning, C. Z. *Nano Lett.* **2009**, *9*, 784−788.
(8) Zhang, Q.; Shan, X. Y.; Zhou, L.; Zhan, T. R.; Wang, C. X.; Li, M.; Jia, J. F.; Zi, J.; Wang, Q. Q.; Xue, Q. K. *Appl. Phys. Lett.* **2010**, *97*, 261107−261109.
(9) Greytak, A. B.; Barrelet, C. J.; Li, Y.; Lieber, C. M. *Appl. Phys. Lett.* **2005**, *87*, 151103−151105.
(10) Hirano, S.; Takeuchi, N.; Shimada, S.; Masuya, K.; Ibe, K.; Tsunakawa, H.; Kuwabara, M. *J. Appl. Phys.* **2005**, *98*, 094305−094311.
(11) Huang, M. H.; Mao, S.; Feick, H.; Yan, H. Q.; Wu, Y. Y.; Kind, H.; Weber, E.; Russo, R.; Yang, P. D. *Science* **2001**, *292*, 1897−1899.
(12) Tamboli, A. C.; Haberer, E. D.; Sharma, R.; Lee, K. H.; Nakamura, S.; Hu, E. L. *Nat. Photonics* **2007**, *1*, 61−64.
(13) Min, B. K.; Ostby, E.; Sorger, V.; Ulin-Avila, E.; Yang, L.; Zhang, X.; Vahala, K. *Nature* **2009**, *457*, 455−U3.
(14) Cho, C. H.; Aspetti, C. O.; Turk, M. E.; Kikkawa, J. M.; Nam, S. W.; Agarwal, R. *Nat. Mater.* **2011**, *10*, 669−675.
(15) Peng, B.; Zhang, Q.; Liu, X.; Ji, Y.; Demir, H. V.; Huan, C. H. A.; Sum, T. C.; Xiong, Q. *ACS Nano* **2012**, *6*, 6250−6259.
(16) Pan, A.; Wang, X.; He, P. B.; Zhang, O. L.; Wan, Q.; Zacharias, M.; Zhu, X.; Zou, B. S. *Nano Lett.* **2007**, *7*, 2970−2975.
(17) Agarwal, R.; Barrelet, C. J.; Lieber, C. M. *Nano Lett.* **2005**, *5*, 917−920.
(18) Qian, F.; Li, Y.; Gradecak, S.; Park, H. G.; Dong, Y. J.; Ding, Y.; Wang, Z. L.; Lieber, C. M. *Nat. Mater.* **2008**, *7*, 701−706.
(19) Nomura, M.; Iwamoto, S.; Watanabe, K.; Kumagai, N.; Nakata, Y.; Ishida, S.; Arakawa, Y. *Opt. Express* **2006**, *14*, 6308−6315.
(20) Nozaki, K.; Kita, S.; Baba, T. *Opt. Express* **2007**, *15*, 7506−7514.
(21) Mahan, G. D. *Phys. Rev.* **1966**, *145*, 602−608.
(22) Dunn, D. *Phys. Rev.* **1968**, *174*, 855−858.
(23) Kena-Cohen, S.; Forrest, S. R. *Nat. Photonics* **2010**, *4*, 371−375.
(24) Tang, H.; Levy, F.; Berger, H.; Schmid, P. E. *Phys. Rev. B* **1995**, *52*, 7771−7774.
(25) Urbach, F. *Phys. Rev.* **1953**, *92*, 1324−1324.
(26) Li, D. H.; Zhang, J.; Zhang, Q.; Xiong, Q. H. *Nano Lett.* **2012**, *12*, 2993−2999.
(27) Zhang, Q.; Zhang, J.; Utama, M. I. B.; Peng, B.; de la Mata, M.; Arbiol, J.; Xiong, Q. H. *Phys. Rev. B* **2012**, *85*, 085418−085426.
(28) Piccione, B.; Cho, C.-H.; van Vugt, L. K.; Agarwal, R. *Nat Nano* **2012**, *7*, 640−645.
(29) van Vugt, L. K.; Piccione, B.; Agarwal, R. *Appl. Phys. Lett.* **2010**, *97*, 061115−061117.
(30) Piccione, B.; van Vugt, L. K.; Agarwal, R. *Nano Lett.* **2010**, *10*, 2251−2256.
(31) van Vugt, L. K.; Piccione, B.; Cho, C. H.; Nukala, P.; Agarwal, R. *Proc. Natl. Acad. Sci. U.S.A.* **2011**, *108*, 10050−10055.
(32) Casperson, L. W.; Khoshnevissan, M. *J. Appl. Phys.* **1994**, *75*, 737−747.
(33) Zimmler, M. A.; Bao, J.; Capasso, F.; Muller, S.; Ronning, C. *Appl. Phys. Lett.* **2008**, *93*, 051101−051103.
(34) Casperson, L. W. *J. Appl. Phys.* **1975**, *46*, 5194−5201.
(35) Pan, A.; Liu, R.; Yang, Q.; Zhu, Y.; Yang, G.; Zou, B.; Chen, K. *J. Phys. Chem. B* **2005**, *109*, 24268−24272.
(36) Zou; Liu, R.; Wang, F.; Pan, A.; Cao, L.; Wang, Z. L. *J. Phys. Chem. B* **2006**, *110*, 12865−12873.
(37) Cheng, K. H.; Zhong, Y.; Xie, B. Y.; Dong, Y. Q.; Hong, Y.; Sun, J. Z.; Tang, B. Z.; Wong, K. S. *J. Phys. Chem. C* **2008**, *112*, 17507−17511.
(38) Duan, X. F.; Huang, Y.; Agarwal, R.; Lieber, C. M. *Nature* **2003**, *421*, 241−245.
(39) Xu, J.; Zhuang, X.; Guo, P.; Zhang, Q.; Huang, W.; Wan, Q.; Hu, W.; Wang, X.; Zhu, X.; Fan, C.; Yang, Z.; Tong, L.; Duan, X.; Pan, A. *Nano Lett.* **2012**, *12*, 5003−5007.
(40) Liao, Z. M.; Wu, H. C.; Fu, Q.; Fu, X. W.; Zhu, X. L.; Xu, J.; Shvets, I. V.; Zhang, Z. H.; Guo, W. L.; Leprince-Wang, Y. M.; Zhao, Q.; Wu, X. S.; Yu, D. P. *Sci. Rep.* **2012**, *2*, 452−457.
(41) Johnson, J. C.; Yan, H.; Yang, P.; Saykally, R. J. *J. Phys. Chem. B* **2003**, *107*, 8816−8828.
(42) Puthussery, J.; Lan, A.; Kosel, T. H.; Kuno, M. *ACS Nano* **2008**, *2*, 357−367.
(43) Reynolds, D. C.; Look, D. C.; Jogai, B. *J. Appl. Phys.* **2000**, *88*, 5760−5763.
(44) Barrelet, C. J.; Greytak, A. B.; Lieber, C. M. *Nano Lett.* **2004**, *4*, 1981−1985.
(45) Liu, X. F.; Wang, R.; Jiang, Y. P.; Zhang, Q.; Shan, X. Y.; Qiu, X. H. *J. Appl. Phys.* **2010**, *108*, 054310−054313.

Supporting information for

“Tailoring the Lasing Modes in Semiconductor Nanowire Cavities using Intrinsic Self-Absorption”

Xinfeng Liu,[1,4 #] *Qing Zhang,*[1, #] *Qihua Xiong* [1, 2, *], *Tze Chien Sum* [1,3,4*]

[1]Division of Physics and Applied Physics, School of Physical and Mathematical Sciences, Nanyang Technological University, Singapore 637371

[2]Division of Microelectronics, School of Electrical and Electronic Engineering, Nanyang Technological University, Singapore 639798

[3]Energy Research Institute @ NTU (ERI@N), Nanyang Technological University, 50 Nanyang Drive, Singapore 637553

[4]Singapore-Berkeley Research Initiative for Sustainable Energy (SinBeRISE), 1 Create Way, Singapore 138602

#These authors contribute to this work equally.

*To whom correspondence should be addressed. Email: qihua@ntu.edu.sg, tzechien@ntu.edu.sg.

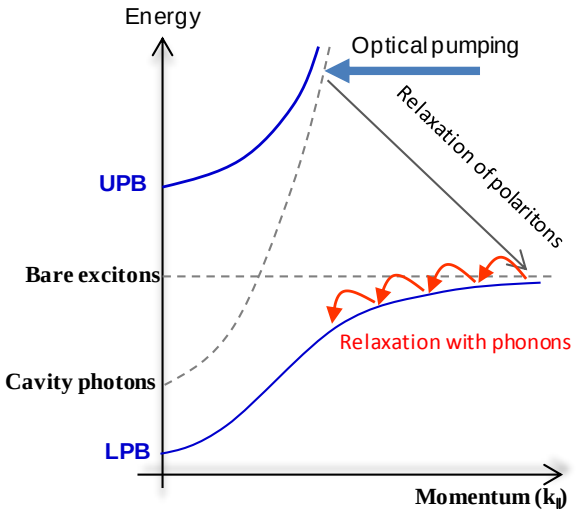

Figure S1. Dispersion curves of cavity photons, bare excitons (dashed lines) and the exciton-polaritons (solid curves). [1]

The curves labeled UPB and LPB are referred to the "upper" and "lower" polariton branches. High energy polaritons from UPB have large photon components in their wavefunctions and will therefore have little interaction with phonons [2]. In this branch, the energy is converted from photons to excitons and vice versa. However, when the polaritons are scattered elastically by defects into the LPB with large exciton components in their wavefunctions, they can lose their energy effectively via scattering with phonons or by nonradiative recombination (e.g., diffusion by electrons). It is predominantly through the latter mechanism that energy in polaritons becomes dissipated inside a medium, resulting in optical absorption.

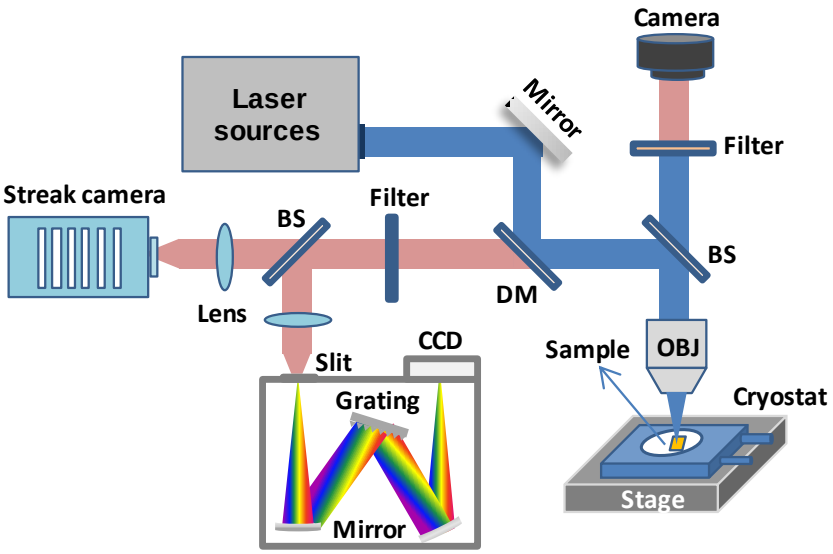

Figure S2. The schematic of the optical setup for measuring the optical properties of single CdS NWs.

A 488 nm diode laser was used as the CW excitation source. For higher density excitation, frequency-doubled pulses (i.e. 400 nm using a BBO crystal) from a regenerative amplifier (1 kHz, pulse width 150 fs, 800 nm) were used. The emission was coupled to either a steady state measurement system (monochromator + CCD) or a time-resolved measurement system (monochromator + streak camera). For the low temperature measurements, a liquid helium continuous flow cryostat (Cryo Industry of America) was used to control the temperature from 20 to 300 K. [Abbreviations: DM: Dichoric Mirror, BS: Beam Splitter, OBJ: Objective, CCD: Charge Coupled Device]

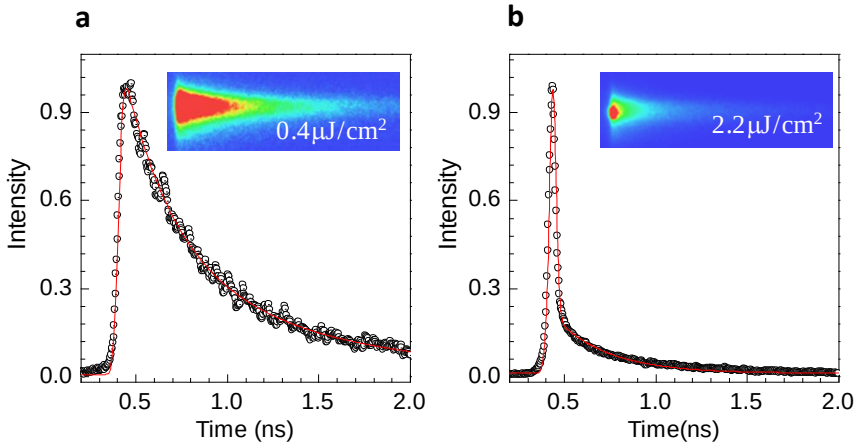

Figure S3. Time-resolved photoluminescence spectra of a single CdS nanowire when laser pump excitation intensity below (a) and above (b) the threshold needed for lasing action, inset are the corresponding streak camera images.

An Optronis Optoscope^{TM} streak camera system (with an ultimate system temporal response of ~ 10 ps) was used to measure the PL lifetimes of single CdS nanowire under different pump excitations (Fig. S3). At pump intensities below the threshold needed for lasing action, the PL lifetime is around 480 ps, matching that of bulk CdS [3]. Above the lasing threshold at 2.2 μJ/cm^2, a dominant lifetime of ~ 10 ps was measured. This even faster lifetime component is due to the lasing action resulting from an avalanche of the radiative recombination, where its lifetime measurement is limited by the system temporal response of the streak camera.

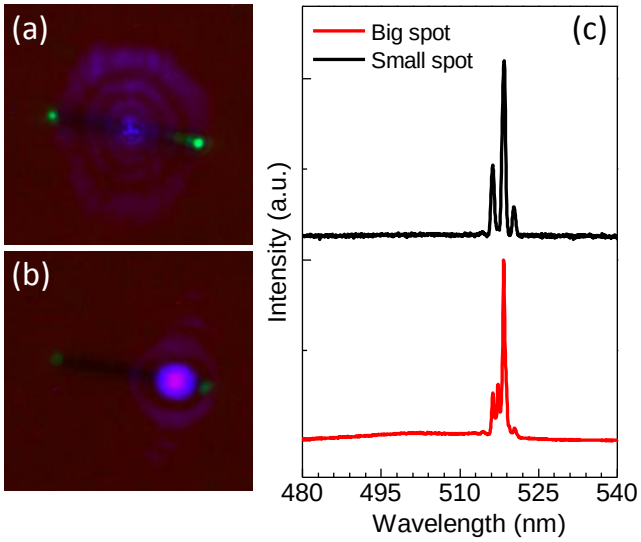

Figure S4. The optical image of a CdS nanowire excited using (a) a large spot size and (b) a small spot size. (c) The corresponding spectra of nanowire excited at (a) and (b).

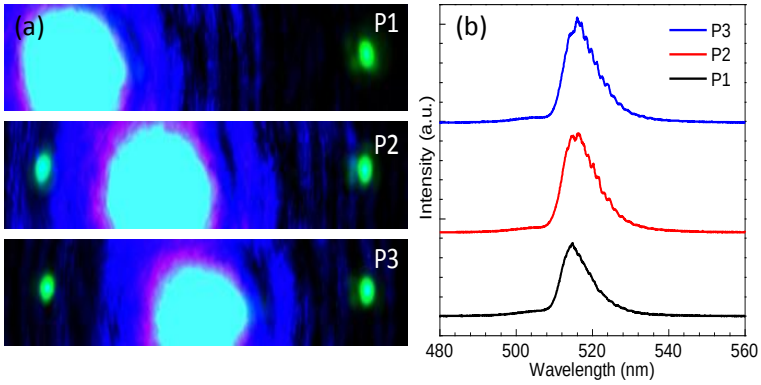

Figure S5. (a) The optical image for a typical CdS NW excited at different positions. (b) The output emission spectra measured at P1, P2 and P3.

We have utilized a larger laser spot size to achieve more efficient energy injection, and to minimize damage to the samples with a tightly focused laser spot. However, we have to highlight that the PL lasing and F-P modes of any nanowire is strongly dependent on its cavity length and the temperature; but have less dependence on the parameters of the pump source. We feel that even if the nanowire is uniformly pumped, the emission from the nanowire will still undergo waveguiding between the two nanowire end facets and self-absorption will still occur. Mode selectivity by the nanowire cavity occurs according to F-P cavity resonance condition. In a nanowire

waveguide, the observed lasing emission is mainly from the two nanowire ends due to the out-coupling arising from the discontinuity of refractive index. Such lasing emission distribution along the entire nanowire can be clearly seen in Figure 2 in our original manuscript.

To substantiate our above points, we have also conducted the following experiments. Firstly, let us address the issue of uniform excitation. It is inherently very difficult to obtain a truly uniform beam that allows full coverage of the NW. But if we use two contrasting beam spot sizes, one should still be able to see the differences in the FP mode positions if uniform excitation does play a crucial role. We demonstrate this with the following cases: (i) a spot size with a FWHM giving > 50% coverage of the NW length; and (ii) a very tightly focused laser beam at one end of the nanowire. The optical images are shown in Figure S4 (a) and (b), respectively. Both spectra are red-shifted with respect to the PL emission peak (at ~ 501 nm) and more importantly, there is hardly any difference in the modal positions in this two contrasting cases.

Another experiment to show that uniform excitation would not be a significant factor is to selectively excite the nanowire along different locations with a tightly focused beam and check their emission spectra – see Figure S5 (a). The corresponding emission peaks shown in Figure S5 (b) are almost invariant, signifying that the absorption (loss) occurs inside the nanowire cavity and is not influenced by the excitation location. Therefore, for CdS nanowires with good waveguiding properties, the emission can effectively propagate along the entire nanowire. Re-absorption (loss) occurs regardless of the pump source being uniform or not. The lasing and F-P oscillating modes are mainly dependent on the nanowire cavity.

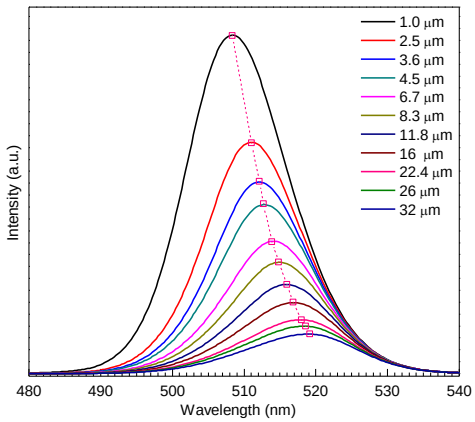

Figure S6. Calculated spectra collected at the emission point and at various positions along the NW from the excitation point.

The pink squares are the peak positions of the emission spectra after propagating through the NW. The relationship between the original intensity $I_0(h\nu)$ and the intensity $I_x(h\nu)$ after propagating a distance, x can be expressed by the equation (1) [4]:

$$I_x(E) = \frac{(1-R)(1-\exp(-x\alpha(h\nu)))}{x\alpha(h\nu)} I_0(E) \qquad (1).$$

where x is the distance between excitation point and the collection point, R is the surface reflectance of the sample and h is Planck's constant, ν is the photon frequency ($E = h\nu$) The expression of $\alpha(h\nu)$ with contributions from the Urbach tail can be expressed as below: $E \geq E_g$,

$$\alpha(E) = A_0 \sqrt{\frac{k_B T}{2\sigma}} \exp\left[\frac{\sigma}{k_B T}\left(E - E_{cr}\right)\right], \qquad (2)$$

$E_{cr} = E_g + k_B T/2\sigma$; *For* $E < E_g$,

$$\alpha(E) = A_0 \exp\left[\frac{\sigma}{k_B T}\left(E - E_g\right)\right] \qquad (3).$$

The values of σ and A_0 were determined in a controlled experiment shown in Figure S7. Based on the experimental data, we obtained the values of 2.0×10^4 and 1 for σ and A_0, respectively.

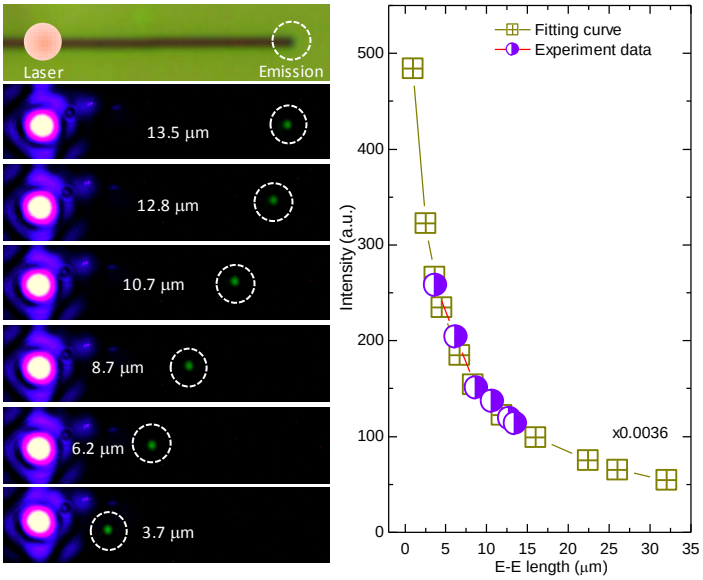

Figure S7. Control experiment to evaluate the value of A_0 and σ.

a, Microscope image and PL microscopy images of a single CdS NW. The NW was excited at different distances from the end facet of the NW. The emission following the waveguiding/transmission through a distance of 13.5 μm, 12.8 μm, 10.7 μm, 8.7 μm, 6.2 μm and 3.7 μm are given in images 2 to 7 in panel a. **b**, The output intensity as a function of propagation length (circles) and the theoretical calculation results (squares), respectively. This theoretical fitting give us the value of A_0 (= 2.0×10^4) and σ (= 1) in equation 1. These values are needed for the evaluation of the CdS NWs absorption coefficient (α).

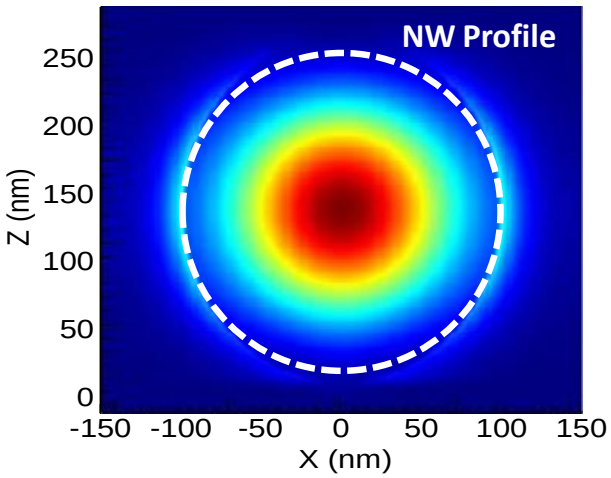

Figure S8. The intensity distribution inside a CdS nanowire, diameter 200 nm, waveguided mode at 505 nm. The result was simulated using the Lumerical Mode Solutions software.

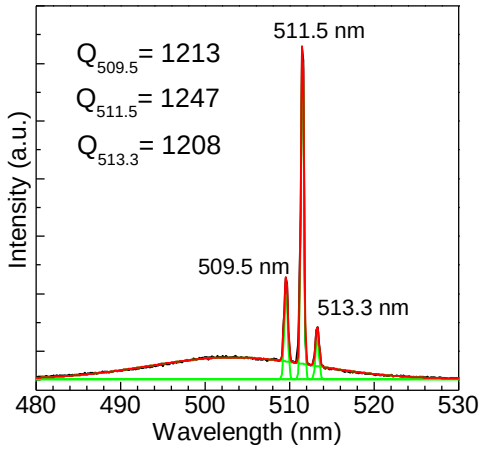

Figure S9. The emission spectra of a CdS nanowire excited with a 400 nm laser at 2.0 µJ/cm2, and the lasing mode at 509.5 nm, 511.5 nm and 513.3 nm are fitted using a Gaussian line shape. Inset gives the Q factors of different modes.

The different guided modes have different mode confinement and hence different "propagation" losses. However considering our nanowire geometry (diameter ~ 200 – 400 nm), which is larger than half the wavelength of the emission propagation inside the nanowire. It is therefore expected that the mode is almost totally confined within the nanowire. Figure S8 presents the FDTD simulation of a guided mode intensity distribution at 505 nm wavelength inside a CdS nanowire of diameter 200 nm. For nanowires with larger diameters, the simulations show that the mode is still well-confined within the nanowire. Consequently, the propagating loss caused by

mode confinement is much weaker than the self-absorption in our system.

We agree that the propagation loss is dependent on the nanowire diameter, crystal structure, surface morphology, doping and even strain, etc. These topics are very interesting. However, our experiment was carefully designed to focus on the self-absorption. Firstly, the CdS nanowires are grown under the same conditions, thus it is reasonable that the crystal structure and surface morphology are similar for the nanowires. Secondly, we have also characterized the nanowires using SEM, TEM and optical spectroscopy. The nanowires show very good crystallinity. Since the modes are well-confined within the nanowire cavity, the mode loss caused by the surface morphology can be neglected.

Furthermore, to quantify the mode propagation loss in the nanowires, we can make use the Q factor of the mode as a comparison. The Q factor is defined as $\lambda/\Delta\lambda$ for a typical F-P cavity [5], where λ is the resonant frequency, $\Delta\lambda$ is the half-power bandwidth. Figure S9 shows the lasing spectra of one typical CdS nanowire. The lasing modes at 509.5 nm, 511.5 nm and 513.3 nm are fitted using Gaussian lineshapes, and the corresponding Q factors are 1213, 1247 and 1208, respectively. This shows that within the 30 nm range (498 nm to 520 nm), the propagation losses of the different modes are comparable. Based on the above considerations, we had concluded that "self absorption" loss is the main factor in our experiments and is highly dependent on the nanowire length.

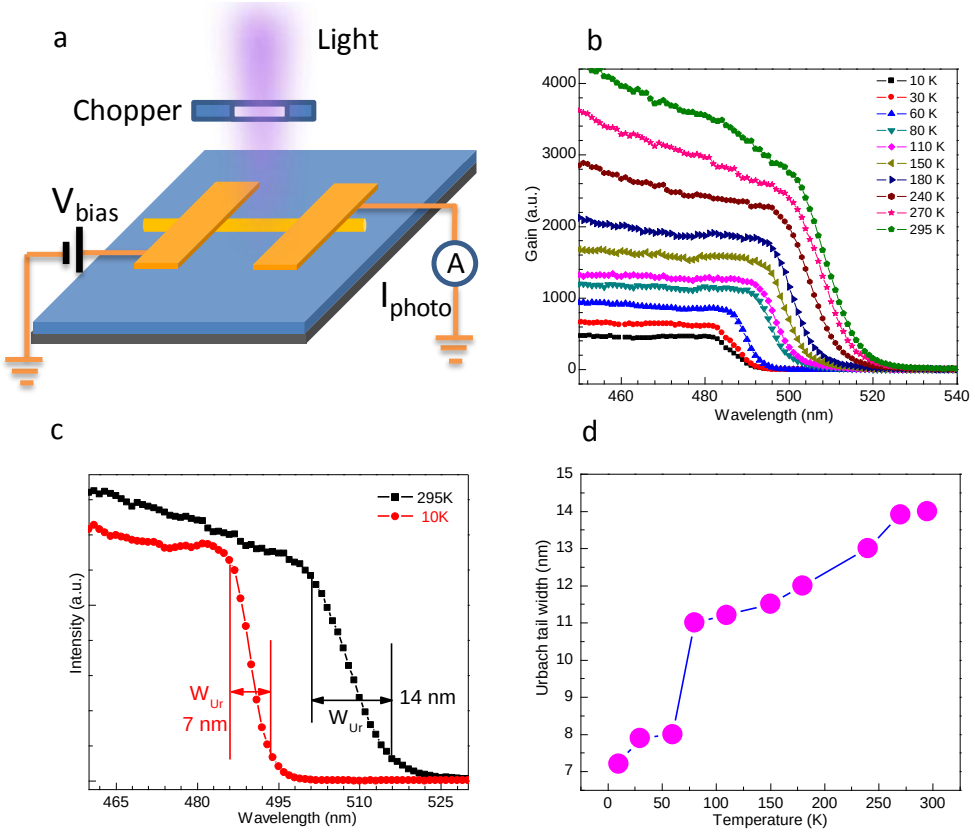

Figure S10. Photoconductivity (I_{ph}) of a CdS NW field-effect transistor (FET) device. a, Schematic of the experimental setup. **b,** The gain of the NW devices at different temperatures. To exclude the influence of incident photon flux fluctuations on the photocurrent, the gain is measured instead. It is defined as the number of electrons collected by electrodes from each incident photon, i.e., $G = (I_{ph}/e)/\phi_{ph}$, where I_{ph} is the photocurrent and ϕ_{ph} is the photo flux). The applied source-drain electric field is 2 kV/cm [6]. **c,** To clearly compare the absorption behavior, we define the width of the Urbach tail as W_{Ur} (the distance over which the gain value falls from 90 % of its central value to 10%). The values of W_{Ur} are 7 nm and 14 nm at temperature of 10 and 295 K, respectively. **d,** Temperature dependence of the Urbach tail width (W_{Ur}) of the CdS NW device.

Strictly, the photocurrent spectrum shown in Fig. S10 depends on both the carrier generation and carrier transport to the electrodes. Therefore, the photocurrent spectrum is related but not exactly equivalent to the optical absorption spectra. Nonetheless, the photocurrent spectrum can still be used to study the electro-absorption if the transport of photo-generated carriers is efficient regardless of the photon energy. Here, these photocurrent spectra are used to estimate the effect of temperature on the Urbach tail. From the photoconductivity results (d in Fig. S10), it is clear that the Urbach tail broadens with increasing the temperature. These results clearly show that the redshift

due to the Urbach tail is indeed suppressed at low temperatures.

References:

[1] H. Deng, G. Weihs, C. Santori, J. Block, Y. Yamamoto, Science **298**, 199-202 (2002)

[3] P. Y. Yu, M. Cardona: Fundamentals of Semiconductors: Physics and Materials Properties (Springer, 2010, Fourth Edition), Chap. 6, p. 283.

[3] J. I. Pankove: Optical Processes in Semiconductors (Dover, New York, 1971), Chap. 6, p. 127.

[4] G. D. Thomas, J. J. Hopfield, Optical properties of bound exciton complexes in Cadmium Sulfide. Phys. Rev. **128,** 2135-2148 (1962).

[5] K. Vahala, Optical microcavities, Nature **424**, 839-846 (2003).

[6] D. H. Li, J. Zhang, Q. Zhang, Q. H. Xiong, Electric-field-dependent photoconductivity in CdS nanowires and nanobelts: exciton ionization, Franz-Keldysh, and Stark effects, Nano Lett. **12**, 2993-2999 (2012).